Local and global effects of boundaries on optical-pattern formation in Kerr media

F. Papoff, G. D'Alessandro,* G.-L. Oppo, and W. J. Firth
Department of Physics and Applied Physics, University of Strathclyde, Glasgow G4 0NG, Scotland
(Received 3 February 1993)

The space-time field evolution in a Kerr slice with single feedback mirror is considered. A full symmetry analysis of the governing equations reveals profound differences between plane-wave and Gaussian-beam excitation. For Gaussian-beam pumping primary bifurcations to a succession of polygonal figures are predicted and confirmed in numerical simulations. Secondary bifurcations are complicated by competition between local and global bifurcations. Chaotic itinerancy and intermittency are among the phenomena observed in the simulations. For broad pump beams, multispot polygons with fivefold symmetry are observed to coexist with sixfold quasilattice patterns, in excellent agreement with the theoretical predictions based on symmetry considerations only.

PACS number(s): 42.65.−k, 05.45.+b, 47.20.Ky

I. INTRODUCTION

Spatial pattern formation in the transverse profile of laser beams propagating in passive media, in presence or in absence of optical cavities, has been recently studied both theoretically and experimentally [1]. Macroscopic symmetries provide a unifying approach to pattern formation in physical systems that differ a great deal on microscopic scales. In general, bifurcation sequences to different stable solutions are observed by changing control parameters [2,3]. Spatial structures associated with these solutions bear either the full symmetry of the system or a lower one corresponding to a subgroup of the full symmetry. The symmetry analysis allows one to separate model-dependent and model-independent features [4], and provides a guideline for an accurate comparison of theoretical models and experiments. Here, for example, we are able to supply predictions about the spatial structure of observable solutions of a model by just considering its overall symmetry.

In this paper, we study pattern formation in the transverse profile of a laser beam propagating through a thin slice of Kerr medium and reflected back by a mirror after propagation in vacuum [6]. We adopt the same governing partial differential equations previously used to study the case of plane-wave input beams [6]. Here we specify different boundary conditions corresponding to a laser beam with a Gaussian intensity profile. Our main result is that transverse boundary conditions modify the symmetry of the solutions with a deep influence on the observed spatial structures.

In the case of plane-wave pumps, the system is invariant under translations, reflections, and rotations in the transverse plane, and has therefore a symmetry corresponding to the Euclidean group E_2. In these situations, narrow intense channels of light (filaments) are formed above the instability threshold of the uniform state. These filaments arrange themselves on grids that break the symmetry E_2 but retain a discrete translational symmetry. Typical examples are rolls and lattices of squares or hexagons, only the latter being stable in the Kerr slice [6].

In contrast, boundary conditions that take into account the Gaussian intensity profile of real laser beams force the system to be invariant under rotations and reflections in the transverse plane only, the symmetry being reduced to the O_2 group. This allows for the observation of solutions in which the filaments form polygonal structures corresponding to the subgroups D_l (l being an integer) of O_2. Such solutions cannot be observed in the plane-wave limit case.

Symmetry properties depend upon the governing partial differential equations and upon the boundary conditions [5]. For large aspect ratio systems, it is generally believed that boundary conditions do not play a relevant role [3]. This is not the case, however, for systems with small aspect ratio in the transverse plane, i.e., the large majority in optics. Therefore, in order to explain the spatial structures arising in experiments, it is important to know how effective the boundary conditions are in the process of pattern formation. The results presented below suggest that spatial patterns in many experiments performed with Gaussian beams should be interpreted in terms of the rotational symmetry only.

The paper is organized as follows. In Sec. II, we introduce the model and discuss its symmetries. In Sec. III, we review some mathematical properties of systems with symmetry and use them to forecast the possible bifurcations. Section IV provides the numerical computations and their comparison with the theoretical predictions. Concluding remarks in Sec. V link our considerations with previous experimental results.

II. THE MODEL

In this section, we briefly review the model equations derived in [6] and describe the propagation of a coherent field in a thin slice of Kerr material in front of a mirror. The equations are

$$\partial_z F = i\frac{\chi}{L} nF \ , \quad \partial_z B = -\frac{\chi}{L} nB \ , \tag{1}$$

$$-\nabla_\perp^2 n + \partial_t n + n = |F|^2 + |B|^2 \ , \tag{2}$$

for the propagation in the nonlinear Kerr medium, and

$$\partial_z F = \frac{i\sigma}{2d}\nabla_1^2 F \ , \quad \partial_z B = -\frac{i\sigma}{2d}\nabla_1^2 B \ , \tag{3}$$

for the propagation in vacuum to and from the feedback mirror. F and B are the forward and backward complex electric fields, n is the excitation density of the medium, χ is the susceptibility, σ is a parameter that measures the relative strength of diffraction versus diffusion (σ is small for strong diffusion), L is proportional to the transverse slice dimension, and d is proportional to the distance of the mirror from the slice. All the variables are adimensional, the lengths being rescaled by the diffusion length and the time by the recombination time of the excitations. We suppose that the field frequency is far from resonance and that the diffusion length is much larger than the wavelength; therefore we do not consider absorption of radiation in the medium or interference between backward and forward fields. Moreover, the slice is considered antireflected to eliminate cavity effects, and thin enough to neglect diffraction inside the medium.

Physically, the origin of the formation of nontrivial spatial structures can be traced in the conversion of the phase modulation of F by the medium [Eq. (1)] into an amplitude modulation of B via the propagation to and from the mirror [Eq. (3)]. Equations (1)–(3) are supplied with transverse and longitudinal boundary conditions. More specifically, we impose the forward field to be equal to the input beam at the entrance of the slice [$F(z=0)=F_{\text{in}}$], the excitation density to be confined within the slice (no flux conditions for n), and the backward field to be proportional to the forward field at the mirror.

In order to apply group-theoretical methods to the analysis of the bifurcations, we need to know the group of symmetries of this model. This means to find all those transformations that map (local) solutions of Eqs. (1)–(3) with specified boundary conditions into other solutions of the same equations. We recall that there are groups of continuous transformations, containing the identity, called connected (e.g., rotations), and also groups of discrete symmetries, such as reflections. For instance, the group O_2 of orthogonal transformations of the plane is composed of the connected subgroup SO_2 of rotations, parametrized by an angle, and of the discrete subgroup D_1, which is made up of the identity and of the reflection with respect to one axis. The O_2 group itself is then not connected. By applying the systematic computational method described in [7], we can find all the connected symmetries arising from transformations of the form

$$g_\epsilon \circ (\mathbf{x},\mathbf{u}) = (\Xi_\epsilon(\mathbf{x},\mathbf{u}), \Psi_\epsilon(\mathbf{x},\mathbf{u})) = (\mathbf{x}',\mathbf{u}') \ , \tag{4}$$

where $\mathbf{x}$ are the independent variables of (1)–(3) (i.e., time and space coordinates), $\mathbf{u}$ are the dependent variables (in our case F, B, and n), and ϵ is a parameter of the group. If $\mathbf{u}=f(\mathbf{x})$ is a solution of (1)–(3), then $g_\epsilon f$ is a solution.

The method consists in finding the infinitesimal generators of the group of symmetries, from which the actual form of Eq. (4) is derived by integration of a set of ordinary differential equations [7]. We discuss here the symmetries of each equation and of the boundary conditions, without showing the explicit calculations, which are straightforward but extremely lengthy. The symmetries that determine the nature of the bifurcations are those common to Eqs. (1)–(3) and to the boundary conditions. Note that it is necessary to follow the systematic calculations presented in [7] in order to guarantee the detection of all the connected symmetries present in the model. An analysis based on an incomplete set of symmetries would lead to spurious bifurcations and, for our purposes, to the prediction of patterns that cannot be observed numerically or experimentally.

The connected group of symmetries for the propagation in vacuum given by Eq. (3) is formed by the following subgroups of transformations

$$T_3 \circ (x,y,z,F) = (x+\epsilon_1, y+\epsilon_2, z+\epsilon_3, F) \ , \tag{5}$$

$$SO_2 \circ (x,y,z,F) = (x\cos\epsilon_4 - y\sin\epsilon_4 \ , \ x\sin\epsilon_4 + y\cos\epsilon_4, z, F) \ , \tag{6}$$

$$R_1 \circ (x,y,z,F) = (e^{\epsilon_5}x, e^{\epsilon_5}y, e^{2\epsilon_5}z, F) \ , \tag{7}$$

$$U_1 \circ (x,y,z,F) = (x,y,z,e^{i\epsilon_7}F) \ , \tag{8}$$

and analogously for B, where we have omitted the trivial symmetries associated with linear combinations of solutions reflecting the linear character of Eq. (3). The symmetry group T_3 represents the translational invariance due to the constant coefficient of the derivatives in Eq. (3); SO_2 gives the invariance under rotation in the transverse plane, which reflects the scalar nature of the operator ∇_1^2; R_1 represents a scaling invariance; U_1 is the phase invariance that corresponds to rotations of the real and imaginary parts of the field.

Equations (1) and (2) are invariant under transformations of the groups T_3, T_1 (time translations), SO_2 (rotations in the transverse plane), and U_1 (phase invariance for the fields). To these connected groups we must add the discrete group D_1 (reflections with respect to one axis and the identity), lifting the spatial symmetry from SO_2 to O_2. Analogously, the field symmetry is lifted from $U(1)$ to the group of unitary 2×2 matrices $U(2)$.

Notice that Eqs. (5)–(8) do not mix independent and dependent variables. This is usually not the case for the Navier-Stokes equations. This in turn shows that there are limitations in the analogy between optical and hydrodynamical systems.

We can easily see that with any relevant choice of boundary conditions, the symmetry related to translations along the propagation direction z is removed and the $U2$ transformations of the fields F and B must be identical. When F_{in} is a plane wave, the model is invariant under rotations, reflections, and translations in the plane transverse to the propagation direction z, while when F_{in} has a Gaussian intensity profile, the model is invariant under rotations and reflections only. From now on, we shall use the compact form

$$\partial_t \mathbf{u} = G(\mathbf{u};\mu) \tag{9}$$

to represent Eqs. (1)–(3), where $\mathbf{u}$ is the set of dependent variables (F,B,n), μ is a generic control parameter, and $G(\mathbf{u};\mu)$ is a nonlinear differential operator.

III. GENERAL REMARKS ON SYMMETRY BREAKING

From the theoretical point of view, problems with Gaussian beams are difficult to handle because analytical forms of the steady state for generic pump shapes are usually unknown. It is in this kind of situation that group theory is particularly useful. For example, in this paper we are able to predict the possible bifurcating solutions and their spatial structure by using symmetry considerations only. More detailed information, such as the stability of the solutions and the subcritical or supercritical character of the bifurcations, has been obtained later by numerical simulations. Symmetry provides the right framework for the numerical analysis because it allows interpretation of the results and checks of their validity, an extremely useful tool when dealing with partial differential equations. Before entering the details of our analysis, we provide a short list of the main results of this section, i.e., the effects of the O_2 symmetry in pattern formation.

(1) The steady-state bifurcations obtained by changing one control parameter (codimension one) from a state with the full O_2 symmetry generate states whose spatial patterns have an overall dihedral symmetry D_l and may sometimes locally look like lattices of hexagons. The integer l, specifying the number of sides of the polygon, depends on the model and on the control parameters. These bifurcations are pitchfork bifurcations.

(2) There exist secondary bifurcations of codimension one, which break the symmetry D_l. For every l, these secondary bifurcations give rise to rotating patterns [8] or to stationary solutions with spatial symmetry D_k, k being a factor of l.

(3) There exist codimension-two mode-mode interactions between patterns with different l values, originating a complex sequence of bifurcations [9].

(4) Patterns with different l may have heteroclinic connections resulting in aperiodic intermittency among the patterns. This is a "global" effect in the sense that symmetry has implications on the stable and unstable manifolds of the solutions of D_l symmetry.

The stationary solutions of (9) are given by

$$G(\mathbf{u};\mu)=0 \ . \tag{10}$$

The bifurcation problem corresponds to the identification of their stability domain and to the characterization of the solutions outside the boundaries. The action of the O_2 group on the domain of Eq. (9) and on a generic function f can be derived from Eq. (6):

$$g_\alpha \circ \theta=\theta+\alpha \ , \quad k\circ\theta=-\theta \ , \tag{11}$$

$$g_\alpha \circ f(\theta)=f(\theta-\alpha) \ , \quad k\circ f(\theta)=f(-\theta) \ , \tag{12}$$

where $\alpha\in[0,2\pi)$ and k represents inversions. Formally, the O_2 symmetry of our system means that, for any element $\gamma\in O_2$, we have

$$\gamma\circ G(\mathbf{u};\mu)=G(\gamma\mathbf{u};\mu) \ . \tag{13}$$

It follows immediately from this equation that if $\mathbf{u}$ is a solution of (10), then also $\gamma\mathbf{u}$ is a solution of (10) for any $\gamma\in O_2$. Whenever $\mathbf{u}$ is not invariant under all the operations of O_2 (i.e., it is a broken-symmetry solution), there is an entire family of solutions $\gamma\mathbf{u}$ obtained from $\mathbf{u}$ and called conjugate solutions. This has important consequences in the study of secondary bifurcations, as we will see in the following of this paper.

The linear stability analysis of a solution $\mathbf{u}$ of (10) with respect to a square integrable perturbation $\mathbf{v}$, such that $\mathbf{u}+\mathbf{v}$ is also a solution of the governing equations, can be studied by taking the Fréchet derivative

$$G_{\mathbf{u}}(\mathbf{u};\mu)\mathbf{v}\equiv\lim_{\epsilon\to 0}\frac{G(\mathbf{u}+\epsilon\mathbf{v};\mu)-G(\mathbf{u};\mu)}{\epsilon} \ . \tag{14}$$

The Fréchet derivative is a linear operator and, in practice, can be performed as a partial derivative with respect to $\mathbf{u}$.

We begin with the primary steady-state bifurcations of a solution $\mathbf{u}_0$ that has the full symmetry of the system and therefore depends only on the radial variable r. The linear stability operator $G_{\mathbf{u}_0}(\mathbf{u}_0;\mu)$ depends on the unknown function $\mathbf{u}_0$ and commutes with all the operations of O_2, as can be seen easily by differentiating (13). Then, the linear stability problem is

$$G_{u_0}(\mathbf{u}_0;\mu)\mathbf{v}=\lambda\mathbf{v} \ , \tag{15}$$

and the bifurcations are obtained by requiring the real eigenvalue λ to vanish. By applying a generic operator γ of the O_2 group to Eq. (15) and by using the commutativity of the operator $G_{\mathbf{u}_0}(\mathbf{u}_0;\mu)$, we obtain

$$\gamma\circ G_{\mathbf{u}_0}(\mathbf{u}_0;\mu)\mathbf{v}=G_{\mathbf{u}_0}(\mathbf{u}_0;\mu)\gamma\circ\mathbf{v}=\lambda\gamma\circ\mathbf{v} \ . \tag{16}$$

From Eqs. (15) and (16), it is clear that the eigenspace E_0 of $G_{\mathbf{u}_0}(\mathbf{u}_0;\mu)$ at the zero eigenvalue is invariant under the operation of the group of symmetry O_2. More precisely, the eigenfunctions of $G_{\mathbf{u}_0}(\mathbf{u}_0;\mu)$ associated with the eigenvalue $\lambda=0$ form a basis of an irreducible representation of O_2 in the subspace E_0. In our case, Eq. (15) takes the form

$$\partial_z\hat{F}-i\frac{\chi}{L}(n^0\hat{F}+F^0\hat{n})=\lambda\hat{F} \ , \tag{17}$$

$$\partial_z\hat{B}+i\frac{\chi}{L}(n^0\hat{B}+B^0\hat{n})=\lambda\hat{B} \ , \tag{18}$$

$$\partial_z\hat{F}-i\frac{\sigma}{2d}\nabla_\perp^2\hat{F}=\lambda\hat{F} \ , \tag{19}$$

$$\partial_z\hat{B}+i\frac{\sigma}{2d}\nabla_\perp^2\hat{B}=\lambda\hat{B} \ , \tag{20}$$

$$\nabla_\perp^2\hat{n}-\hat{n}+(F^0\hat{F}^*+B^0\hat{B}^*+\text{c.c.})=\lambda\hat{n} \ , \tag{21}$$

where $\mathbf{u}_0=(F^0,B^0,n^0)$ and $\mathbf{v}=(\hat{F},\hat{B},\hat{n})$, with the previously specified boundary conditions [11]. We recall that $\mathbf{u}_0$ is unknown, but it does not depend upon the angular coordinate. By using cylindrical coordinates, one can see that functions $\mathbf{v}$ of the type $\mathbf{R}_l(z,r)\sin(l\theta)$ and $\mathbf{R}_l(z,r)\cos(l\theta)$ are solutions of Eqs. (17)–(21), which are then reduced to a system of partial differential equations for the axial variable z and the radial variable r, with the

index l^2 to be fixed. Note that $\mathbf{R}_l(z,r)\sin(l\theta)$ and $\mathbf{R}_l(z,r)\cos(l\theta)$ provide a basis for an irreducible representation of O_2, which is two dimensional if $l\neq 0$ and one dimensional if $l=0$ [10]. Generically, a codimension-1 bifurcation will involve only one irreducible representation of O_2 [12], corresponding to a single value of l. From the angular dependence of the eigenfunctions of E_0, we can see that the two-dimensional eigenspace is invariant under rotations of multiples of $2\pi/l$, corresponding to the subgroup S_l of O_2. Notice that $\mathbf{R}_l(z,r)\cos(l\theta)$ is a one-dimensional linear subspace of E_0, which is invariant under the inversion $\theta\rightarrow -\theta$, and that the only element of E_0 that is invariant under the full symmetry group O_2 is $\mathbf{R}_l(z,r)=0$. In general, apart from highly degenerate cases, the spectrum of eigenvalues of the operator $G_{\mathbf{u}_0}(\mathbf{u}_0;\mu)$ is identical to that of its adjoint [in this case, $G_{\mathbf{u}_0}(\mathbf{u}_0;\mu)$ is said to be a Fredholm operator of order 0]. Then, by assuming that this condition holds for our case, we can use the result of [13] and state that there is a branch of solutions $\mathbf{u}_l$ whose spatial structure has the symmetry of the dihedral subgroup D_l.

These solutions are contained in a subspace X^{D_l} such that the operations of D_l act as the identity transformation in this subspace. The bifurcation problem can then be reduced to this subspace. It is important to notice that this subspace is invariant under the action of elements of the subgroup D_{2l}, which is larger than D_l. Moreover, the elements of D_{2l} commute with the elements of D_l and may be separated in two classes containing the elements that belong (do not belong) also to D_l. These two classes operate on X^{D_l} as D_1 so that the bifurcations are basically governed by the action of D_1. We can then use the results of [14] and state that these bifurcations are symmetric pitchfork bifurcations, where the two secondary branches are conjugate. Moreover, considering that the leading nonlinearities of (9) are quadratic and that the product of cosines is again a combination of cosines, we can see that on one branch of the bifurcation, $\mathbf{u}_l$ has the form $\sum_{m=0}^{\infty}\mathbf{R}_{ml}(z,r)\cos(ml\theta)$. Rotations of an angle $\alpha\in(0,2\pi/l)$ generate distinct conjugate solutions. Rotations of an angle π/l, which belongs to D_{2l} but not to D_l, originate solutions on the other branch of the bifurcation, of the form $\sum_{m=0}^{\infty}(-1)^m\mathbf{R}_{ml}(z,r)\cos(ml\theta)$. The original O_2 symmetry, which is not shown by any of these solutions, is recovered when considering the whole family of solutions with spatial structure symmetric under D_l. Notice that when $l=0$, the bifurcations do not break the symmetry.

We briefly outline here the results of Ref. [8], which apply to secondary bifurcations of systems with a subgroup of the main symmetries isomorphic to the group SO_2 of rotations. As we have seen, for any solution $\mathbf{u}_l$ of Eq. (10) with dihedral symmetry D_l, there is a family of solutions $g_\alpha\mathbf{u}_l$ obtained by rotating $\mathbf{u}_l$. The total derivative with respect to the angular variable α on the left-hand side of Eq. (13) is

$$\left.\frac{dG(g_\alpha\circ\mathbf{u}_l;\mu)}{d\alpha}\right|_{\alpha=0}=G_{\mathbf{u}_l}(\mathbf{u}_l;\mu)\circ\left.\frac{d(g_\alpha\circ\mathbf{u}_l)}{d\alpha}\right|_{\alpha=0}=0. \quad (22)$$

From Eq. (22), we can see that the system is neutrally stable along the direction of the family of solutions. This happens because the linear stability operator $G_{\mathbf{u}_l}(\mathbf{u}_l;\mu)$ has eigenvectors $d(g_\alpha\mathbf{u}_l)/d\alpha$ tangent to the family of solutions $g_\alpha\mathbf{u}_l$, corresponding to the eigenvalue $\lambda=0$. A bifurcation of the family of solutions $g_\alpha\mathbf{u}_l$ occurs if the operator $G_{\mathbf{u}_l}(\mathbf{u}_l;\mu)$ has an eigenvalue on the imaginary axis whose eigenvector is not tangent to the family of solutions. The dynamics of the system can then be separated into the directions parallel and perpendicular to the family of solutions $g_\alpha\mathbf{u}_l$. Mathematically, this means that the operator $G(\mathbf{u}_l;\mu)$ of Eq. (9) can be split in an operator $G^T(\mathbf{u}_l;\mu)$ and an operator $G^N(\mathbf{u}_l;\mu)$, operating along the directions tangent and normal to the family of solutions, respectively. An interesting phenomenon can happen in this case: bifurcations in the normal direction will produce spatial structures drifting along the direction parallel to the family of solutions $g_\alpha\mathbf{u}_l$. Therefore, a steady-state bifurcation can excite a frequency in the system, in our case a rotation in the transverse plane. A Hopf bifurcation can thus excite two frequencies, one being the usual frequency associated to the imaginary part of the eigenvalue, the other corresponding to the rotation in the transverse plane. The possible bifurcations depend on how the group of symmetry D_l of the bifurcating solution $\mathbf{u}_l$ acts on the subspace E_0^N of the eigenvectors of the operator $G_{\mathbf{u}_l}^N(\mathbf{u}_l;\mu)$ corresponding to the eigenvalue $\lambda_0^N=0$. According to theorem (6.1) of Ref. [8], the only possible secondary bifurcations of solutions $\mathbf{v}_l$ are the following.

(1) Conjugate branches of rotating waves if the subspace E_0^N is invariant under the action of the subgroup S_l of D_l.

(2) Conjugate branches of steady-state solutions with spatial symmetry D_m $(m=l/2)$ if the subspace E_0^N is invariant under operations isomorphic to the subgroup D_m of D_l.

(3) Two nonconjugate branches of steady-state solutions with spatial symmetry D_i, where i is a factor of l different from $l/2$ and 1, if the subspace E_0^N is invariant under the action of the subgroup S_i of D_l corresponding to rotations of $2\pi/i$.

A similar theorem is provided in Ref. [8] for Hopf bifurcations. We found numerically bifurcations corresponding to each of the cases listed above.

So far we have discussed local effects of the symmetry in the neighborhood of bifurcations. There are also global effects of symmetry, which may produce heteroclinic connections among families of solutions corresponding to different symmetries D_l. These heteroclinic connections are associated with chaotic or periodic trajectories starting from the neighborhood of a family of solutions and exploring successively regions of phase space close to other families, before eventually coming back close to the initial condition. As the symmetry of the system determines the presence of invariant subspaces in the phase space, heteroclinic cycles connecting different families of solutions are, in general, more common in systems with symmetry. Moreover, the robustness of these cycles is

enhanced by symmetry, as transversal connections between stable and unstable manifolds are no longer a requisite for their existence. Note also that heteroclinic cycles have strong effects on the dynamics even when unstable [18]. Heteroclinic connections have also been studied for the interaction between two modes obtained through primary steady-state bifurcations in the presence of O_2 symmetry in [15]. In optics, heteroclinic connections in interaction among three modes obtained through primary Hopf bifurcations with imperfect O_2 symmetry have been used [16] to explain the chaotic and periodic alternation observed experimentally in Ref. [17]. In our system, we found numerically chaotic itinerancy among solutions emerging from primary as well as secondary bifurcations. To our knowledge, a theoretical analysis of this case is still lacking, but it should be possible following the lines of Refs. [18,15,16].

In Sec. IV, we show by numerically integrating Eqs. (1)–(3) that spatial structures with the dihedral symmetry are stable for large regions of the parameter space whenever Gaussian input laser beams are considered. Moreover, secondary bifurcations of the kind described above, as well as global behavior leading to intermittency, have been detected and their effects on the dynamics of the solutions analyzed. It must be stressed here that all the predictions made above have been based on symmetry considerations and not on specific knowledge of the solutions of Eqs. (1)–(3).

IV. NUMERICAL ANALYSIS

We have performed numerical simulations of Eqs. (1)–(3) using input beams with a Gaussian intensity profile. We have used a hopscotch method [19] on a two-dimensional grid of 256×256 lattice points. Convergence has been assured by taking the ratio between the time step and the square of the mesh size smaller than 0.25. In order to organize the bifurcation trees, we have used two control parameters: The beam waist and the maximum intensity of the input beam. We found bifurcations from solutions with the full O_2 spatial symmetry into solutions with dihedral symmetry, in agreement with the general symmetry predictions of Sec. III. More precisely, we first observed a steady-state bifurcation that does not break the symmetry from purely Gaussian profiles into Gaussian-like structures with circular rings in their tails. Then, by changing the control parameters, another steady-state bifurcation occurs, leading to solutions with spatial structure with dihedral symmetry D_l with $l=2,3,5,6$. The number of filaments increases by increasing the beam waist of the pump, and multistability among these patterns has been observed. The near and far fields of these spatial structures are shown in Figs. 1 and 2. Notice that whenever the beam waists are small enough, the patterns corresponding to D_2, D_3, D_5, and D_6 have 4, 3, 6, and 7 filaments, respectively. In some cases, it is difficult to discriminate between different patterns by using the far-field images only. For example, the far-field images of the D_2, D_3, and D_6 structures are remarkably similar to regular hexagons, but, when studied in detail, Fig. 1(c) shows a D_2 symmetry only, while Fig.

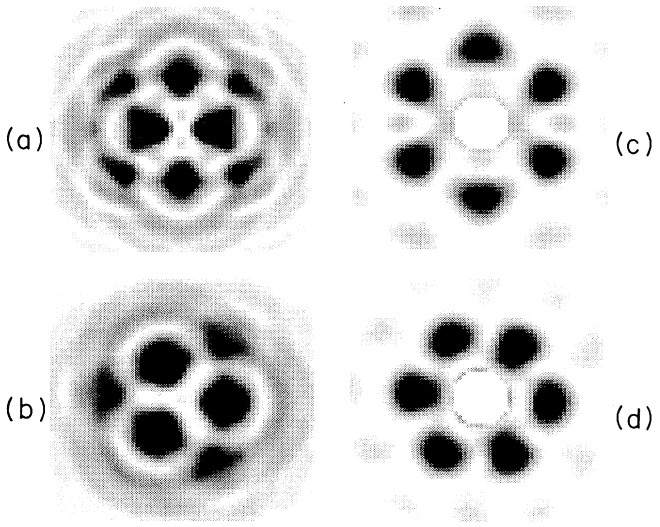

FIG. 1. Center region of the beam (64×64 lattice points) is displayed in this figure and in the following ones. Panels (a) and (c) show the near- and far-field distributions of a solution with symmetry D_2, for $\sigma=10$, $I=2.7$, $\eta=1.92$, where I is the ratio between the maximum intensity and the threshold intensity for the plane-wave case, and η is the ratio between the input beam waist and the critical length for the patterns obtained with a plane-wave input beam. In (b) and (d), we show the near- and far-field distributions of a solution with symmetry D_3 for $\sigma=10$, $I=2.2$, $\eta=1.80$. In the far-field images, the central peak has been removed following the experimental procedure [22].

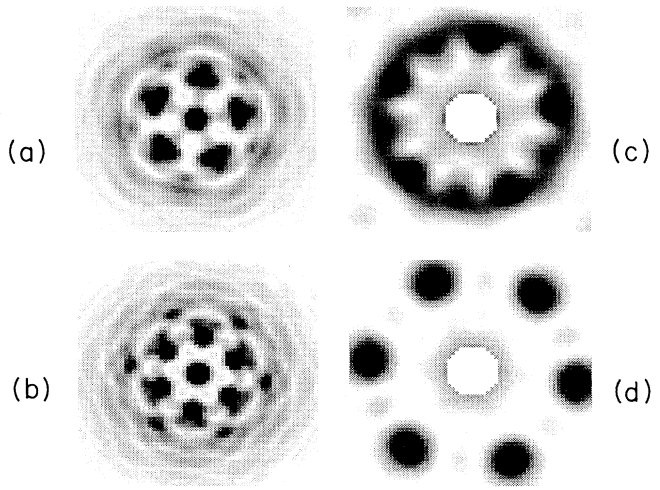

FIG. 2. Panels (a) and (c) show the near- and far-field distributions of a solution with symmetry D_5 for $\sigma=10$, $I=2.2$, $\eta=2.40$. In (b) and (d), we show the near- and far-field distributions of a solution with symmetry D_6 for $\sigma=10$, $I=2.2$; $\eta=2.64$. In the far-field images, the central peak has been removed following the experimental procedure [22].

1(d) shows a D_3 structure, being the superposition of two triangles. These differences in the far-field patterns may be difficult to observe experimentally. However, the assessment of the correct symmetry of the spatial structure is of fundamental relevance in determining the subsequent bifurcation tree, and near-field images are preferable.

For small values of the beam waist, we observed secondary bifurcations in which the spatial structures D_3 are slightly deformed and start to rotate slowly. From the list of possible secondary bifurcations of codimension one given in Sec. III, we know that the only possible secondary steady-state bifurcations of a solution with spatial symmetry D_l (with l being a prime integer) lead to rotating waves. As the rotation depends basically on the presence of a continuous family of solutions with spatial symmetry D_3 (a consequence of the rotational symmetry of the system), this bifurcation may disappear if the rotational symmetry is perturbed by either optical misalignments in experiments or square grids in numerical simulations. The detection of this bifurcation, therefore, can provide a good test about the robustness of the O_2 symmetry to perturbations.

For the D_2 spatial structures [Fig. 1(a)], we have observed secondary symmetry-breaking bifurcations to metastable structures with symmetry D_1, shown in Fig. 3(a). In our simulations, solutions with D_1 symmetry are metastable, so that after some time they break into rotating filaments. Note that the initial transition from D_2 to D_1 is one of the two possible codimension-1 bifurcations, the other being a bifurcation into rotating patterns.

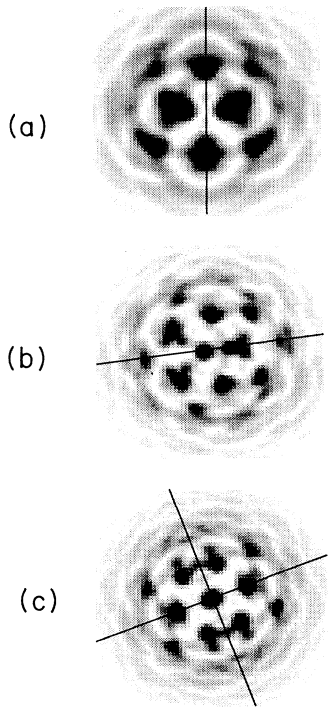

FIG. 3. (a) Structure with symmetry D_1, which emerged from a solution with symmetry D_2 for $\sigma=10$, $I=2.72$, $\eta=1.92$. (b) Structure with symmetry D_1, which emerged from a solution with symmetry D_5 for $\sigma=10$, $I=2.7$, $\eta=2.40$. (c) Structure with symmetry D_2, which emerged from a solution with symmetry D_2 for $\sigma=10$, $I=2.3$, $\eta=2.64$. The straight lines show the symmetry axes.

For the D_5 spatial structures [Fig. 2(a)], we have observed bifurcations to structures with symmetry D_1 also [see Fig. 3(b)]. As the latter structure is unstable in our simulations, the laser intensity oscillates among solutions that have imperfect (yet recognizable) symmetries of the D_1, D_3, and D_5 type. In this case, the only possible codimension-one bifurcation would originate rotating structures, which, however, have not been observed in our extensive numerical simulations.

For the D_6 spatial structures [Fig. 2(c)], we have observed secondary bifurcations to a D_2 spatial structure [see Fig. 3(c)], which has not been found in primary bifurcations. This is followed by irregular itinerancy among structures with imperfect symmetry D_1, D_4, and D_6. Because of the complexity of the spatiotemporal evolution, details about this kind of transition are available on video cassettes. Note that the initial transition from D_6 to D_2 is one of the three possible codimension-one bifurcations, the other two being transitions to D_3 symmetric structures and to rotating solutions. This behavior indicates a nontrivial interplay between codimension-one secondary symmetry-breaking bifurcations of local nature and heteroclinic cycles. In our case, spatial structures of type D_1 and D_4 have been generated via secondary bifurcations only, while D_3, D_5, and D_6 came from primary bifurcations. This situation has not been studied in the existing literature, and we envisage a future generalization of the normal-form theory presented in Ref. [15] in order to include our case.

We now select the control parameters so as to have a stable spatial structure with dihedral symmetry D_l. By increasing the waist of the input laser beam and by decreasing its maximum intensity, it is possible to increase the total number of filaments of the solutions, preserving the overall symmetry D_l. In Figs. 4(a) and 4(b), for example, we show a D_5 and a D_6 structure made up by three different pentagons and hexagons, respectively, one inside the other. These spatial structures are stable in our numerical simulations for times as long as 200 units on the time scale of the excitation density. The number of filaments on the pentagons is $5m$ and on the hexagons is $6m$, where m is an integer index such that the m_0th structure contains all the structures with $m < m_0$ and is contained in all the structures with $m > m_0$. This is in agreement with the form of the D_l solutions given in Sec. III in terms of cosines. Locally, the outer filaments arrange themselves on small hexagons around the core of the spatial structure. In the case of the D_5 spatial structure shown in Fig. 4(a), there is a pentagon at its core surrounded by deformed hexagons. In contrast to what happens in systems with translational invariance, the pentagon here is not a defect, but is part of a spatial structure with symmetry D_5, which can be stable. Analogously, the D_6 spatial structure of Fig. 4(b) looks like part of an hexagonal lattice, but its origin is a pitchfork bifurcation and not a transcritical bifurcation typical of systems with

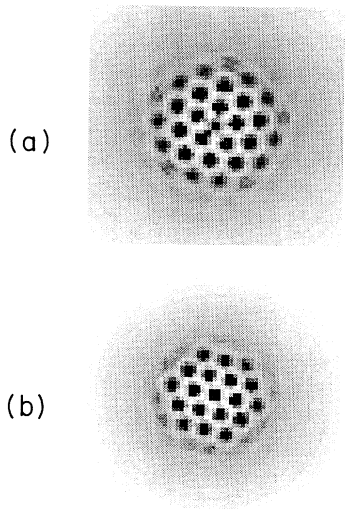

FIG. 4. Spatial structures with a large numbers of filaments with symmetry D_5 for $\sigma=10$, $I=1.23$, $\eta=5.52$ (a) and D_6 for $\sigma=10$, $I=1.28$, $\eta=6.00$ (b).

translational invariance [6]. Moreover, we observed a wide region of bistability between these two spatial structures for large enough beam waists. In this region, we found also a continuous competition between a pentagon and a hexagon at the core of the spatial structure, while the outer region remains unmodified. The experimental observation of these patterns may not be easy but, nevertheless, our results show that the breaking of the translational invariance induced by the transverse boundaries is relevant for wide input beams as well as for small ones.

If the pump intensity is increased quickly, we do not observe the formation of rings in the tails of the Gaussian profile, and filaments appear initially at random positions in the transverse profile of the beam. Whenever new filaments are created, they move and rearrange themselves so as to form ordered structures, usually with a dip in the center.

V. CONCLUSION

In this work, we have shown that pattern formation in laser beams propagating in Kerr media with feedback mirror is deeply changed when taking into account the Gaussian intensity profile of the input beams. Although in some cases the far field looks like a hexagon, the associated patterns are not necessarily hexagons, and the dynamics may change drastically from case to case. In fact, we have observed bifurcations to patterns that can be explained only when considering the O_2 and the broken translational symmetries. This means that in order to compare pattern formation in experiments and theoretical models, one has to verify that the underlying symmetries are the same. In particular, we have shown that special care has to be taken whenever the transverse boundary conditions break the translational invariance of the models.

Because of the universality of the symmetry considerations used here, we expect results similar to that of Sec. IV to hold for several optical systems ranging from lasers to counterpropagating beams in gases. For example, there is a striking similarity between Figs. 1(b) and 1(d) and recent experimental results on alkali-metal vapors, either cavityless [20] or in front of a single mirror [21] or in presence of counterpropagation [22]. For all these cases, we believe that the breaking of the translational symmetry is the key ingredient for the formation of dihedral structures. Predictions about changes and dynamical behavior originating from these structures have then to be based on models where the translational symmetry is removed. It is important to point out that, in order to observe O_2 symmetry breaking in experiments without optical cavities, one must check carefully that the pump beams are actually O_2 symmetric. Amplitude or phase distortion can destroy the symmetry, and in that case, the analysis presented here does not hold.

We wish also to stress that symmetry may be useful for understanding to what extent the bifurcations depend upon the model. In the present model, for example, we do not include absorption in the medium. In real experiment, this condition will not be fulfilled, but, as long as the absorption is unsaturable (e.g., band-tail absorption), this should affect only the position of the primary bifurcations to solutions with spatial structure D_n. When the absorption is saturable, a new time scale appears in the problem and the primary bifurcations could be Hopf bifurcations. Finally, the overall symmetry and its action on the governing equations changes whenever the susceptibility χ is a tensor that depends on the spatial variables. In this case, entirely new bifurcations could appear.

ACKNOWLEDGMENTS

We wish to thank G. K. Harkness, A. J. Scroggie, H. G. Solari, and M. A. Vorontsov for useful discussions and suggestions. One of us (F.P.) wishes to thank G. B. Mindlin for sharing information about his work on chaotic itinerancy. This work was partially supported by SERC (Grant No. GR/G 15031) and by the EEC via SCIENCE Grant No. 16325 and an ESPRIT grant (TONICS).

*Present address: Departement de Physique Théorique, Université de Genève, CH-1211, Genève 4, Switzerland.

[1] For an updated list of references, see N. B. Abraham and W. J. Firth, J. Opt. Soc. Am. B **7**, 951 (1990).

[2] C. Green, G. B. Mindlin, E. J. D'Angelo, H. G. Solari, and J. R. Tredicce, Phys. Rev. Lett. **65**, 3124 (1990).

[3] P. Manneville, *Dissipative Structure and Weak Turbulence* (Academic, San Diego, 1990).

[4] M. Golubitsky, I. Stewart, and D. G. Schaeffer, *Singularities and Groups in Bifurcation Theory* (Springer-Verlag, New York, 1988).

[5] J. D. Crawford and E. Knobloch, Ann. Rev. Fluid Mech.

199, 471 (1989).
[6] W. J. Firth, J. Mod. Opt. **37**, 151 (1990); G. D'Alessandro and W. J. Firth, Phys. Rev. Lett. **68**, 3698 (1991); G. D'Alessandro and W. J. Firth, Phys. Rev. A **46**, 537 (1992).
[7] P. J. Olver, *Applications of Lie Groups to Differential Equations* (Springer, New York, 1986).
[8] M. Krupa, SIAM J. Math. Anal. **21**, 1453 (1990).
[9] G. Dangelmayr and D. Ambruster, Contemp. Math. **56**, 53 (1986).
[10] M. Hamermesh, *Group Theory and its Application to Physical Problems* (Addison-Wesley, Reading, MA, 1962).
[11] Note that, at the entrance of the slice, $\hat{F}=0$ as the input beam is contained in F_0.
[12] P. J. Aston, SIAM J. Math. Anal. **22**, 181 (1991).
[13] G. Cicogna, Lett. Nuovo Cimento **31**, 600 (1981).
[14] M. Dellniz and B. Werner, J. Comp. Appl. Math. **26**, 97 (1989).
[15] D. Armbruster, J. Guckenheimer, and P. Holmes, Physica D **29**, 257 (1988).
[16] F. T. Arecchi, S. Boccaletti, G. B. Mindlin, and C. Perez Garcia (unpublished).
[17] F. T. Arecchi, G. Giacomelli, P. Ramazza, and S. Residori, Phys. Rev. Lett. **65**, 2531 (1990).
[18] D. Ambruster and P. Chossat, Physica D **50**, 155 (1991).
[19] A. R. Gourlay, J. Inst. Math. Its. Appl. **6**, 375 (1970).
[20] J. W. Grantham, H. M. Gibbs, G. Khitrova, J. F. Valley, and X. Jiajin, Phys. Rev. Lett. **66**, 1422 (1991).
[21] G. Giusfredi, J. F. Valley, R. Pon, G. Khitrova, and H. M. Gibbs, J. Opt. Soc. Am. B **5**, 1181 (1988).
[22] A. Petrossian, M. Pinard, A. Maître, J.-Y. Courtois, and G. Grynberg, Europhys. Lett. **18**, 689 (1992).

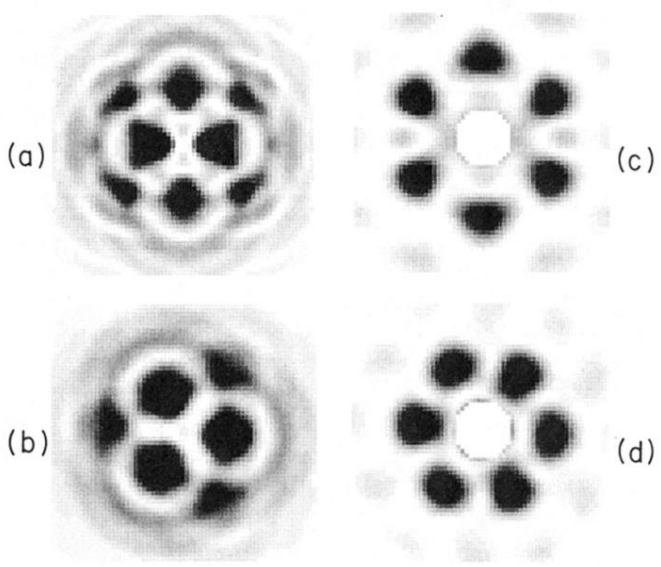

FIG. 1. Center region of the beam (64×64 lattice points) is displayed in this figure and in the following ones. Panels (a) and (c) show the near- and far-field distributions of a solution with symmetry D_2, for $\sigma=10$, $I=2.7$, $\eta=1.92$, where I is the ratio between the maximum intensity and the threshold intensity for the plane-wave case, and η is the ratio between the input beam waist and the critical length for the patterns obtained with a plane-wave input beam. In (b) and (d), we show the near- and far-field distributions of a solution with symmetry D_3 for $\sigma=10$, $I=2.2$, $\eta=1.80$. In the far-field images, the central peak has been removed following the experimental procedure [22].

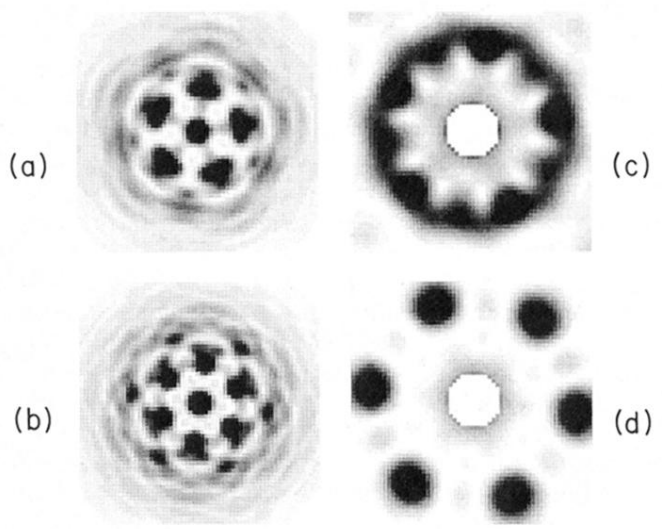

FIG. 2. Panels (a) and (c) show the near- and far-field distributions of a solution with symmetry D_5 for $\sigma=10$, $I=2.2$, $\eta=2.40$. In (b) and (d), we show the near- and far-field distributions of a solution with symmetry D_6 for $\sigma=10$, $I=2.2$; $\eta=2.64$. In the far-field images, the central peak has been removed following the experimental procedure [22].

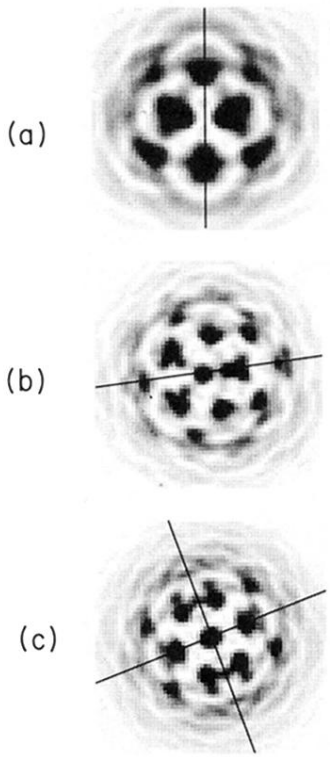

FIG. 3. (a) Structure with symmetry D_1, which emerged from a solution with symmetry D_2 for $\sigma=10$, $I=2.72$, $\eta=1.92$. (b) Structure with symmetry D_1, which emerged from a solution with symmetry D_5 for $\sigma=10$, $I=2.7$, $\eta=2.40$. (c) Structure with symmetry D_2, which emerged from a solution with symmetry D_2 for $\sigma=10$, $I=2.3$, $\eta=2.64$. The straight lines show the symmetry axes.

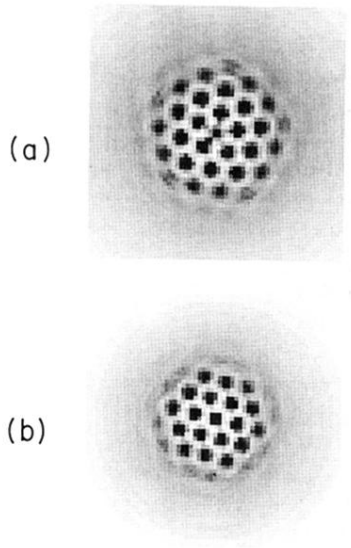

FIG. 4. Spatial structures with a large numbers of filaments with symmetry D_5 for $\sigma=10$, $I=1.23$, $\eta=5.52$ (a) and D_6 for $\sigma=10$, $I=1.28$, $\eta=6.00$ (b).